PROCEEDINGS, 42nd Workshop on Geothermal Reservoir Engineering
Stanford University, Stanford, California, February 13-15, 2017
SGP-TR-212

Subsurface Imaging of Raft River Geothermal Field Using 2010 Walkaway VSP Data

David Li[1], Kai Gao[1], Yunsong Huang[1], Miao Zhang[1], Benxin Chi[1], Joseph Moore[2], and Lianjie Huang[1]

[1]Geophysics Group, Los Alamos National Laboratory, Los Alamos, NM 87545, USA

[2]Energy & Geoscience Institute, University of Utah, Salt Lake City, UT 84108, USA

Emails: davidzli@lanl.gov (David Li), ljh@lanl.gov (Lianjie Huang)

Keywords: Imaging, Raft River, Reverse-Time Migration, Tomography, Vertical Seismic Profile

ABSTRACT

The Raft River geothermal field in southern Idaho is the site of a successful DOE Enhanced Geothermal System demonstration project. Prior to the drilling of sidetrack RRG-9 ST1, the stimulated well, a vertical seismic profile (VSP) survey was conducted in 2010 in the original well to image subsurface structures. The survey included a zero-offset VSP and eight walkaway VSP lines. The VSP data were recorded using 40 three-component receivers in well RRG-9, with a receiver interval of approximately 15 m, located at measured depths from 15 m to 600 m. Vibroseis sources with intervals of approximately 30 m to 60 m were used for the VSP survey. The maximum source offset from the well was around 2 km. To image the subsurface structures, we process the raw VSP data to separate the down-going and up-going wavefields, and build 1D and 2D velocity models using tomographic inversions of the first-arrival times of the down-going waves. We then apply reverse-time migration to the up-going waves of the VSP data and obtain high-resolution subsurface images along the eight walkaway lines at the Raft River geothermal field.

1. INTRODUCTION

The Raft River Geothermal field is located in Cassia County, Idaho and has been used as a field site for Enhanced Geothermal Systems (EGS) studies since the early 1970s. The area mainly consists of a Cenozoic structural basin filled on top with roughly 1600 m of Tertiary sediment (Covington 1980). The geothermal resource in this area comes from a fracture dominated reservoir near the base of this Cenozoic basin fill (Covington 1983). There is also a region of faulting in the basement rock known as the Narrows zone through which heated water flows along to reach the basin reservoir (Covington, 1983). To image these underlying structures, a walkaway VSP survey was conducted in February 2010. The VSP well is the original RRG-9 well drilled in 2006 to a measured depth of 1856 m (Jones et al. 2011). The 2010 Raft River VSP survey consists of 40 three-component receivers placed into well RRG-9 to a measure depth of 600 m and 251 point sources along eight walkaway lines on the surface. The receiver interval is approximately 15 m, and the source interval ranges from 30 to 60 m. The eight walkaway lines are arranged around the well along different azimuths with the receivers at the center. Figure 1 shows the map of the shots and receivers and Fig. 2 shows a cross-section of two walkaway lines.

2. METHOD

To image subsurface structures at the Raft River geothermal site, we first process the three-component (3C) raw VSP data and separate them into the upgoing and downgoing wavefields. We then build 1D and 2D velocity models using 1D least squares inversion and 2D travel time tomography, respectively. Finally we apply reverse-time migration to the separated upgoing wavefields using the 2D velocity model to image the subsurface structures.

Reverse-time migration (RTM) is a full-wavefield imaging method with no limitations in structural dipping angle (McMechan, 1983). It is therefore a powerful tool for imaging complex subsurface structures. Conventionally, prestack RTM can produce a subsurface image using zero time-lag cross-correlation between the source and the receiver wavefields:

$$I(x) = \sum_{N_s, N_r} \int_0^T S(x,t) R(x,t) dt \,, \tag{1}$$

where $S(x,t)$ is the source wavefield and $R(x,t)$ is the receiver wavefield.

It is known that the imaging condition in Equation (1) could be contaminated by low wavenumber artifacts resulting from the cross-correlation between the wavefields propagating in the same direction (Liu et al., 2011). In addition, the imaging condition in Equation (1) is unable to separate the images dominated with horizontally-dipping structures (sedimentary layers) and those dominated with steeply-dipping structures (faults and fractures). To circumvent this problem, we employ RTM imaging conditions based on implicit wavefield separation (Fei et al., 2015):

$$I(\mathbf{x}) = \sum_{N_s, N_r} \int_0^T SR - H_z(S) H_z(R) - SH_z(H_t(R)) - H_z(S) H_t(R) dt \,, \tag{2}$$

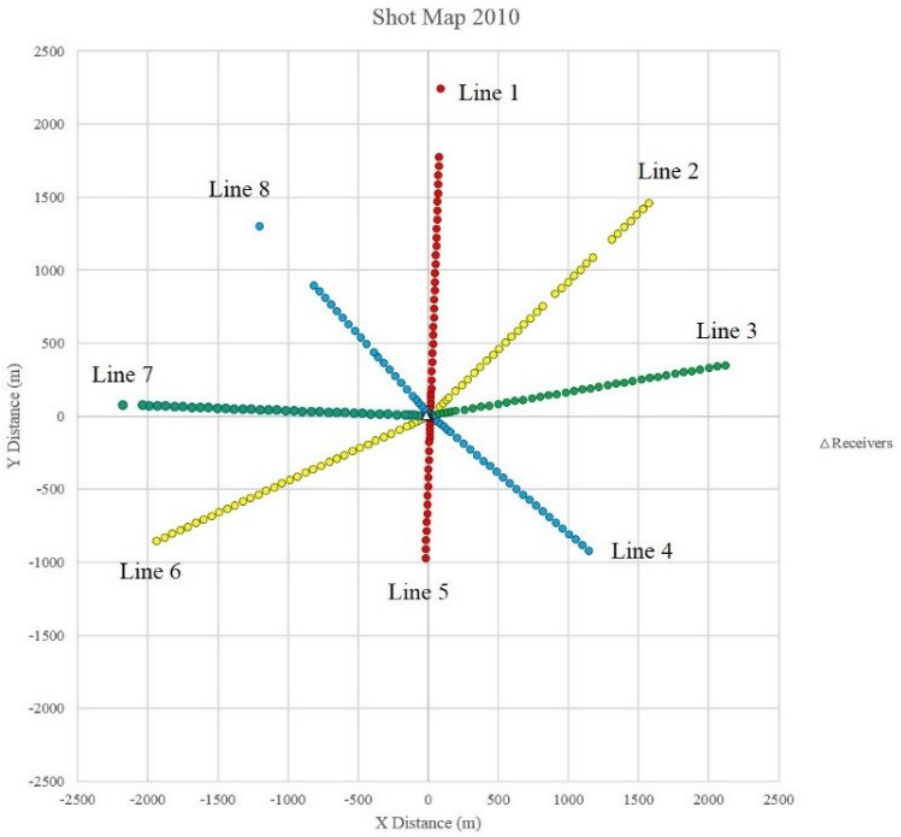

Figure 1: Source and receiver map for the 2010 walkaway VSP survey at the Raft River geothermal field. The walkaway lines are labeled as Lines 1-8.

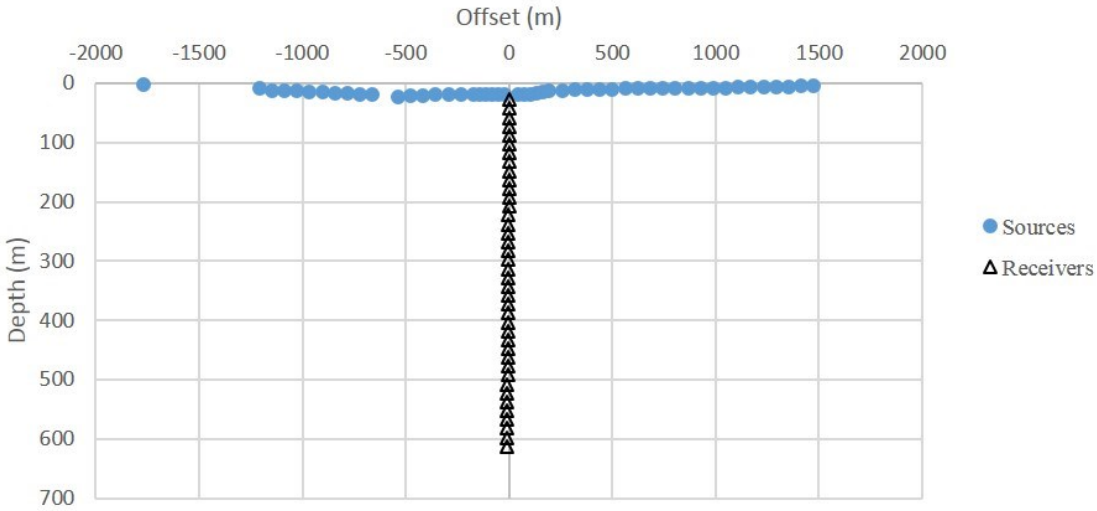

Figure 2: A cross-section view of the source and receiver locations. This figure represents the cross-section view of walkaway line 8 on the left side and line 4 on the right.

where H_t represents the Hilbert transform in the time domain, and H_z represent the Hilbert transforms in the depth direction. The time-domain Hilbert transform is applied to observed seismic traces. The Hilbert-transformed seismic signals are then propagated in a reverse-time manner as the auxiliary sources, together with the reconstructed source wavefield S and reverse-time propagated receiver wavefield R, to produce migration images using Equation (1).

To compensate for the energy loss in the deep region of the model, we normalize the image generated using Equation (2) with the source and receiver wavefield energies:

$$I(\mathbf{x}) = \sum_{N_s} \left(\frac{\sum_{N_r} \int_0^T SR - H_z(S)H_z(R) - SH_z(H_t(R)) - H_z(S)H_t(R)dt}{\left(\sqrt{\sum_{N_r} \int_0^T S^2 dt} + \varepsilon \right) \left(\sqrt{\sum_{N_r} \int_0^T R^2 dt} + \varepsilon \right)} \right), \tag{3}$$

where ε is a tiny value to avoid division by zero. We also apply an appropriate spatial taper for each prestack common-shot image to reduce migration artifacts caused by small numbers of sources and receivers.

3. RESULTS

3.1 Processing of the 3C VSP Data

The raw VSP data collected using vibroseis sources consists of data with a sweep of 24 seconds and a sample rate of 1 millisecond. After correlation, the seismic traces are 6 seconds long. All common-shot gathers contain strong noises in the traces for receivers located at measure depths from 195 m to 270 m. We inspect the amplitude spectra of these traces and find that there is a sharp increase in amplitude at 15 Hz for each of these noisy traces. We employ a 15 Hz notch filter to these traces to successfully remove most of the noise.

We first pick the first-arrival times of the direct arrivals, and use them to rotate the three components of the raw VSP data so that the vertical component is parallel to the direction of the downgoing P waves, and the two horizontal components are orthogonal to the vertical component. After horizontal and vertical rotations of the data, the vertical component is the direct component, the Horizontal 1 component becomes the perpendicular component, and the Horizontal 2 component is denoted as the tangential component. The direct component contains the downgoing P waves and upgoing SV waves, the perpendicular component contains the downgoing SV waves and the upgoing P waves, while the tangential component contains the downgoing and upgoing SH waves. Figure 3 shows three components of a common-shot gather before and after rotation. We then separate the upgoing wavefield from the total wavefield of the perpendicular component to image the structures.

To image subsurface reflectors, we use median filters to separate the weaker upgoing waves from the stronger downgoing waves in the data. We first pick the arrival times of downgoing waves, and apply an 11-point median filter to separate the downgoing waves from the data. We then subtract the downgoing wavefield from the total wavefield to obtain the upgoing wavefield. After subtracting the downgoing wavefield, we then pick an upgoing event and apply another median filter of 7 points to refine the upgoing waves. Figure 4 displays the perpendicular component of a common-shot gather together with separated downgoing and upgoing wavefields.

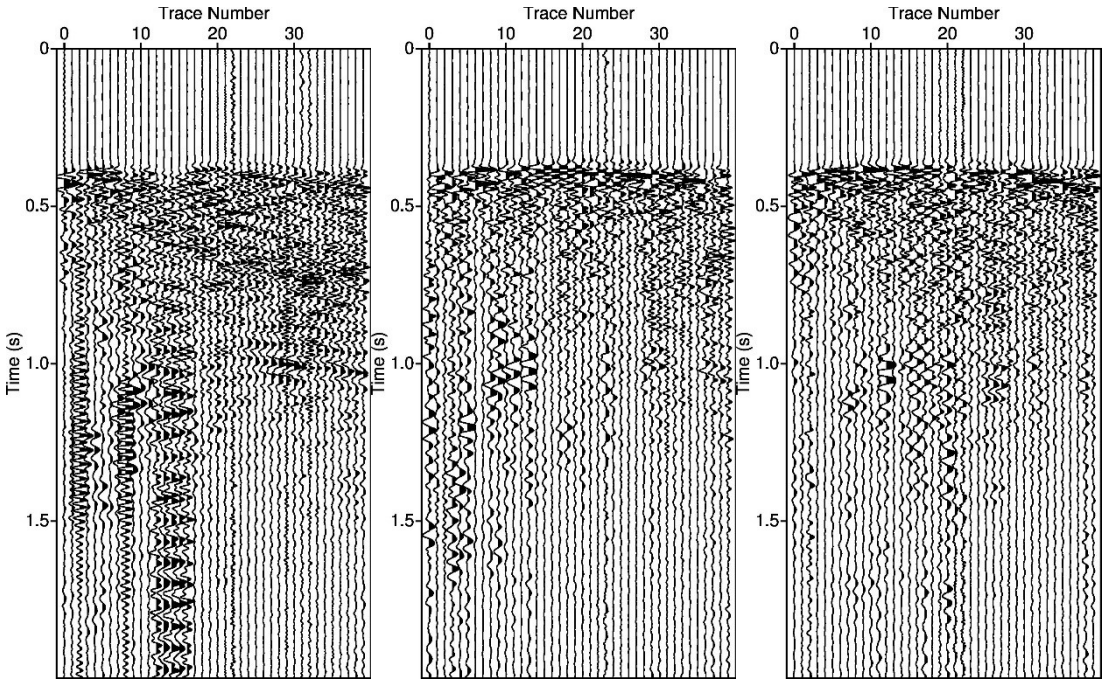

(a)

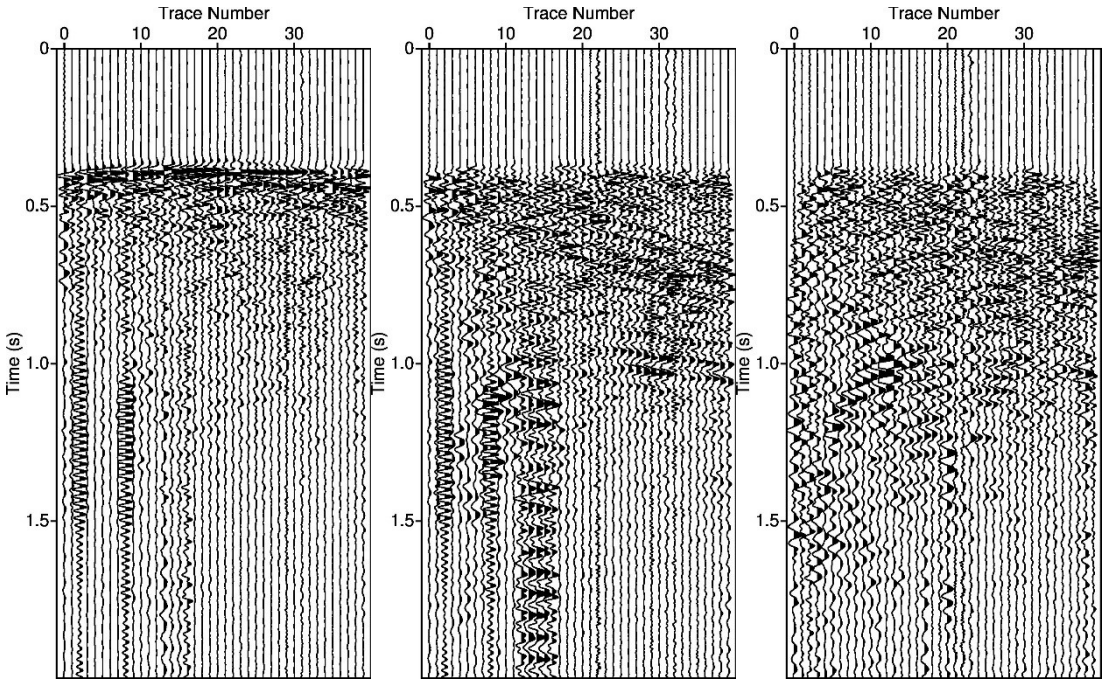

(b)

Figure 3: The VSP data before and after rotation for three components of a common-shot gather for Shot 815. (a) The data before rotation, where the three components are the Vertical (top left), Horizontal 1 (top center) and Horizontal 2 (top right). (b) The data after rotation, where the components are the direct component (bottom left), the perpendicular component (bottom center), and the tangential component (bottom left).

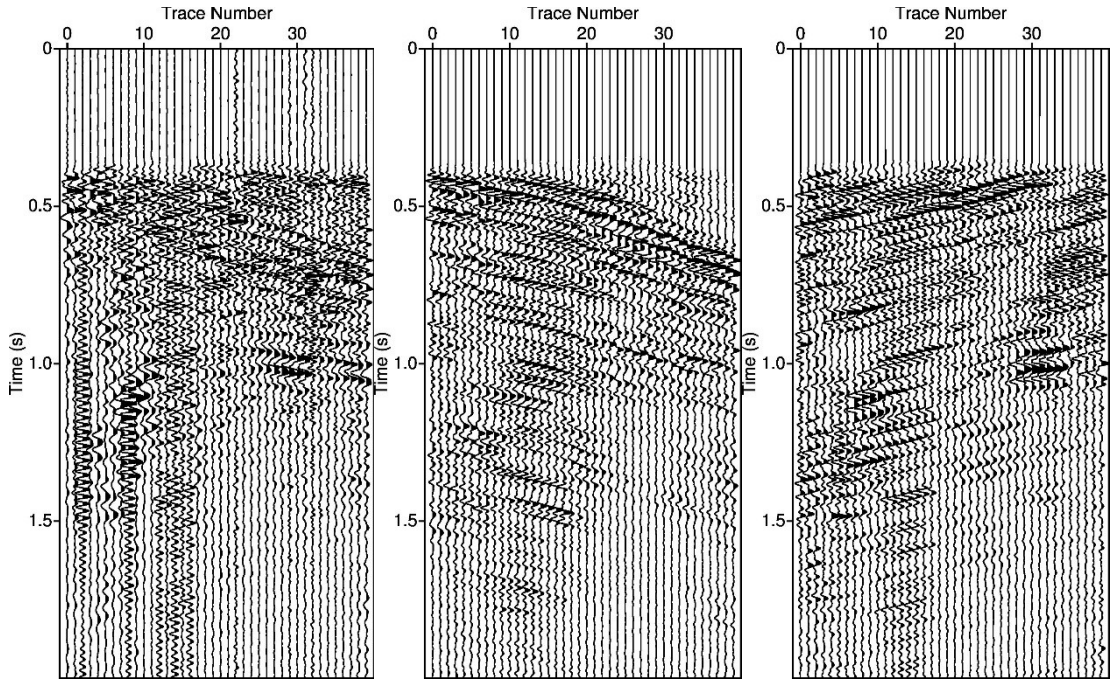

Figure 4: Left panel: The perpendicular component of a common-shot gather for Shot 815. Center panel: The separated downgoing wavefield of the common-shot gather. Right panel: The separated upgoing wavefield of the common-shot gather.

3.2 Building 1D and 2D Velocity Models Using 1D Least Squares Inversion and 2D Travel-time Tomography

We employ a 1D least squares inversion method to build an initial velocity model using the first-arrival times of the downgoing direct waves of the zero-offset VSP data. In the 2010 VSP survey, the deepest receiver in well RRG-9 was located at 600 m in depth, so we only have first-arrival travel times up to 600 m in depth. However, the target imaging zone (Narrows zone) is much deeper than 600 m. We conducted the other VSP survey in May 2016 using the same well where the lowest receiver was placed at a measure depth of deeper than 1500m. The data of the shallow region of the zero-offset VSP data from the 2016 survey are heavily contaminated by noises and unusable. We combine the shallow region of the zero-offset VSP from the 2010 VSP survey with the deeper region of data from the 2016 survey to build a 1D velocity model as shown in the left panel of Fig. 5. We then use this 1D model as an initial model for 2D travel-time tomography, and obtain a 2D velocity model depicted in the right panel of Fig. 5.

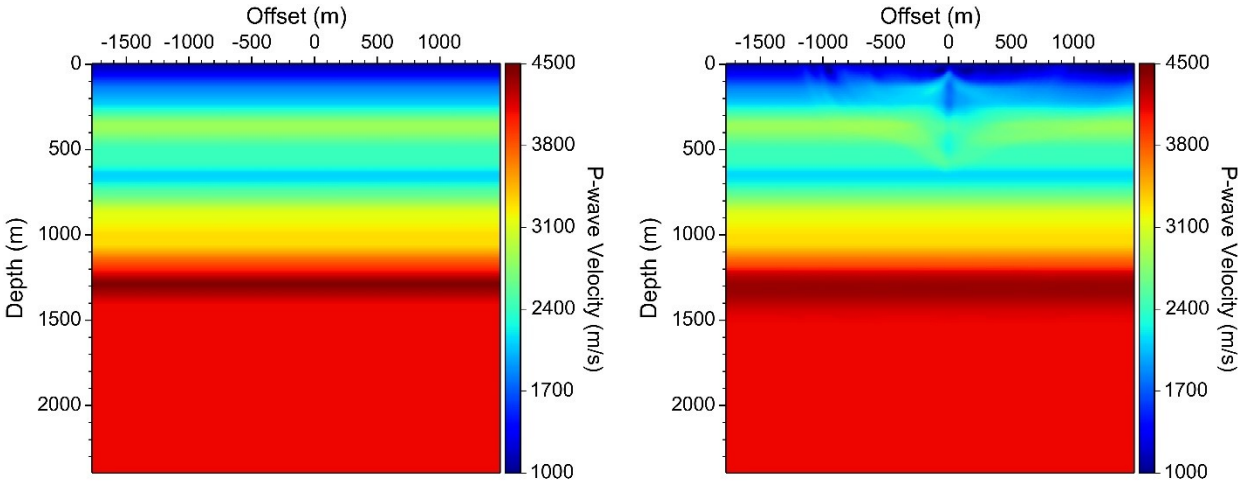

Figure 5: Left panel: The 1D velocity model built using 1D least squares inversion; Right panel: The 2D velocity model of a single walkaway line built using 2D travel-time tomography of downgoing waves.

3.3 Reverse-time migration

We conduct reverse-time migration using separated upgoing wavefields and the 2D velocity model. Figure 6 shows the image of a tied walkaway line. Several reflectors on the image could correspond to some geologic structures. For example, the reflector at depth of approximately 500 m may correspond to the interface between the Raft River Formation and the Salt Lake formation. The continuous event between 1200 m and 1400 m in depth may represent the interface between the Upper Tuff Member and the Jim Sage Volcanic Member of the Salt Lake Formation. Finally, the continuous event near 1600 m may represent the boundary of the Quartz Monzonite. Figure 7 shows the comparison of the reverse-time migration image with a geologic column taken from well RRG-9. (Jones et al. 2011). Four reflectors in the reverse-time migration image are consistent with the real geologic layers shown in the left hand column of the figure.

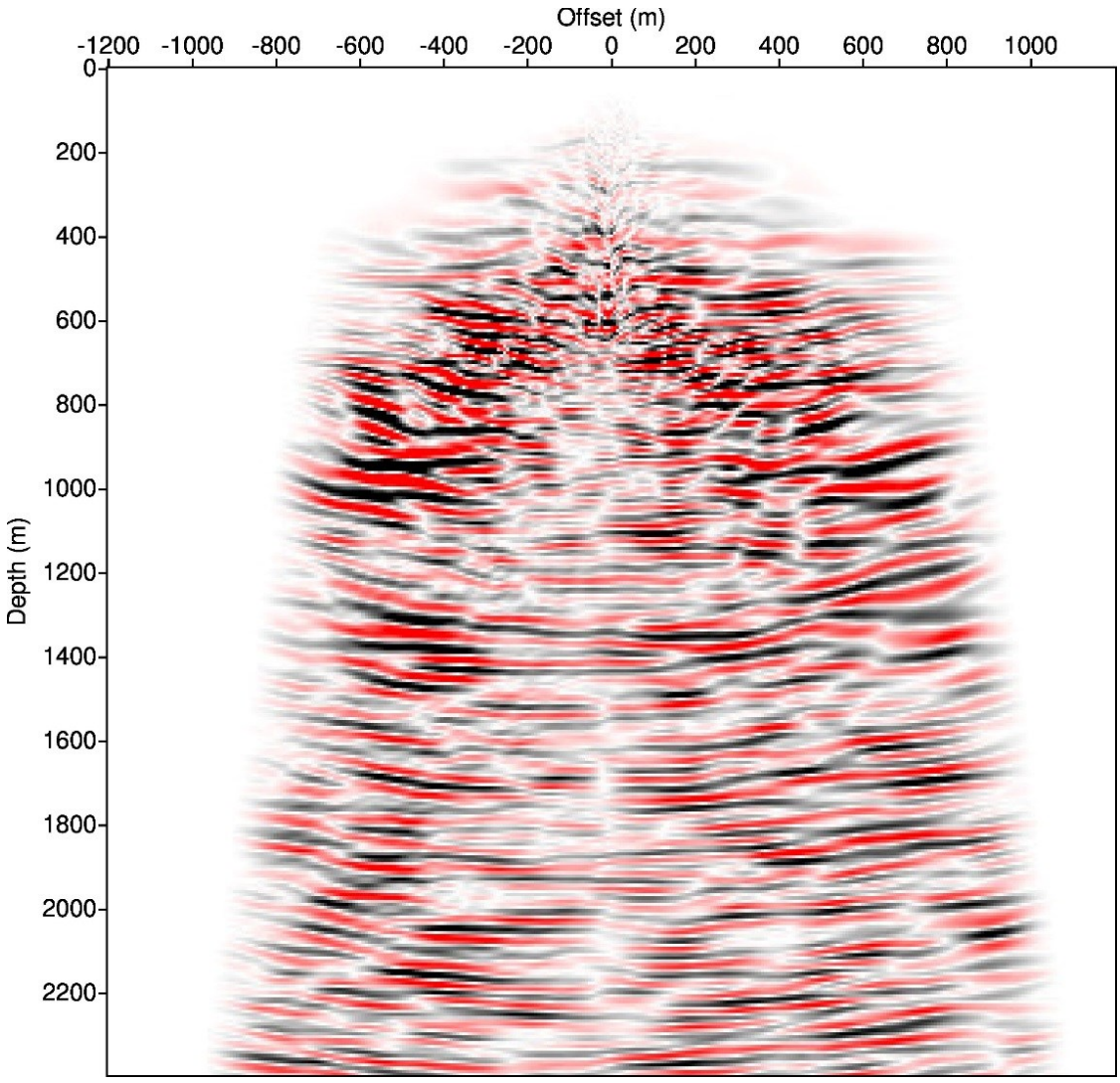

Figure 6: A reverse-time migration image of two walkaway lines for the VSP data acquired at the Raft River geothermal field in 2010.

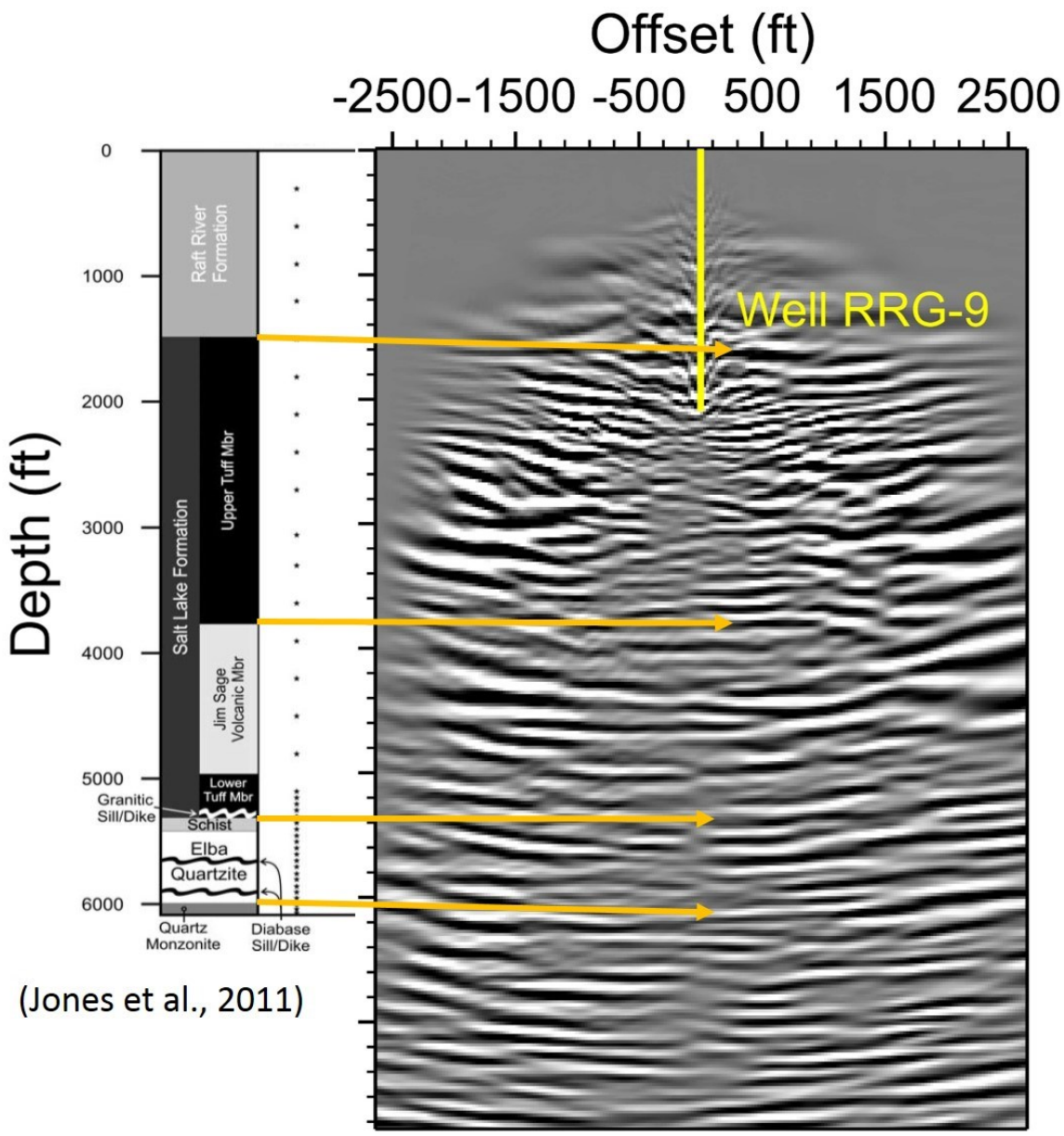

Figure 7: A reverse-time migration image of two walkaway lines for the VSP data acquired at the Raft River geothermal field in 2010. There are four reflections that are consistent with actual geologic features (Jones et al. 2011).

4. CONCLUSIONS

We have successfully processed the raw VSP data acquired at the Raft River geothermal field in 2010 using 40 levels of receiver and eight walkaway source lines. We have obtained high-quality separated upgoing wavefields, constructed a 2D velocity model using tomographic inversion of first-arrival times, and conducted reverse-time migration of the separated upgoing wavefields to image subsurface structures at the Raft River geothermal field. We have found several reflectors from the migration image that may correspond to actual geologic formations.

5. ACKNOWLEDGEMENTS

This work was supported by the Geothermal Technologies Office (GTO) of the U.S. Department of Energy through contract DE-AC52-06NA25396 to Los Alamos National Laboratory. We thank Dr. Yingping Li for his insightful discussions. We acknowledge strong support of GTO Program Managers William Vandermeer, Sean Porse and Lauren Boyd. The computation was performed on super-computers provided by the Institutional Computing Program of Los Alamos National Laboratory.

REFERENCES

Covington, H. R.: Subsurface Geology of the Raft River Geothermal Area, Idaho, *Geothermal Resources Council*, *Transactions,* **4**, (1980), 113-115.

Covington, H.R.: Structural evolution of the Raft River Basin, Idaho, *Geological Society of America, Memoir,* **157**, (1983), 229-237

Fei, T. W., Luo, Y., Yang, J., Liu, H., and Qin, F.: Removing false images in reverse time migration: The concept of de-primary, *Geophysics*, **80**, (2015), S237-S244.

Jones, C., Moore, J., Teplow, W., and Craig S.: Geology and Hydrothermal Alteration of the Raft River Geothermal System, Idaho, Proceedings, 36th Workshop on Geothermal Reservoir Engineering, Stanford University, Stanford, CA (2011)

Liu, F., Zhang, G., Morton, S. A., and Leveille, J. P.: An effective imaging condition for reverse-time migration using wavefield decomposition, *Geophysics*, **76**, (2011), S29-S39.

McMechan, G. A.: Migration by extrapolation of time-dependent boundary values, *Geophysical Prospecting*, **31**, (1983), 413-420.